Steadily Decreasing Power Loss of a Double Schottky Barrier Originating from the Dynamics of Mobile Ions with Stable Interface States

Zhuolin Cheng,[1,‡] Zongke Hou,[1,‡] Yao Wang,[1] Men Guo,[1] Kangning Wu,[1,*] Jianying Li,[1,†] and Ying Lin[2]

[1] *State Key Laboratory of Electrical Insulation and Power Equipment, Xi'an Jiaotong University, Xi'an 710049, China*

[2] *School of Electrical and Automation Engineering, Hefei University of Technology, Hefei 230009, China*

(Received 2 October 2021; revised 9 February 2022; accepted 16 February 2022; published 15 March 2022)

A general aging model of the double Schottky barrier was proposed to unveil the long-term aging behaviors of ZnO varistor ceramics, especially for those ones with steadily decreasing power loss. For those samples, the barrier height and electrical properties were even enhanced rather than commonly deteriorated, which were beyond the classic ion migration model. In this paper, inspired by the unique reversible aging of them, interface states are proposed to remain stable in those samples. The major mobile ions, which have been in debate, are further identified to be $Zn_i^{\cdot}$ ions. Based on these assumptions, a quantitative dynamic ion migration-diffusion model is proposed. The calculated power loss steadily decreases with aging time, which well supported our proposal. When the interface states are not combined with those mobile ions, the formation of a "U-shape" ion spatial distribution in depletion layers is found to be responsible for the unique aging phenomena, i.e., a reduction in the depletion layer and interfacial charge, a rise in the depletion layer width, and an increase in the barrier height. However, continuously increasing power loss would be generated if the mobile ions combined with the interface states. Therefore, a general mechanism on the aging of the double Schottky barrier is unveiled that it is a competition process between consumption of the interface states and the dynamics of mobile ions in depletion layers.

DOI: 10.1103/PhysRevApplied.17.034042

I. INTRODUCTION

Formation of a potential barrier at interfaces is the source of functionalization for numerous functional materials that are widely employed in electrical and electronic devices, such as solar cells [1], detectors [2,3], sensors [4,5], and varistors [6–8]. Specifically, because of excellent nonlinear current-voltage characteristics originated from the double Schottky barrier (DSB) at the grain boundary [9,10], varistor ceramics are widely employed for overvoltage protection with voltage levels ranging from a few volts to millions of volts. However, due to the aging of DSB, degradation of varistors is inevitably generated during the long-term operation, which can cause serious failures to the entire system. Therefore, there is a pressing need to clarify the aging mechanism of DSB, especially in the situation that current understandings lag behind the practical development of varistors [9].

Taking the most widely used ZnO varistor ceramics as an example, they are manufactured by sintering highly pure ZnO power (content >95%) and various metal-oxide dopants, e.g., Bi_2O_3, Sb_2O_3, Co_2O_3, MnO_2, Cr_2O_3 [9]. As varistors, they are connected in parallel to electrical devices, withstanding long-term electrical stress, and more significantly, protecting the devices from overvoltage surges [9,11]. ZnO varistor ceramics can be divided into three types according to their dependences of power loss on aging time [12,13]. They are traditional type I with monotonously increasing power loss, type II with continuously increasing power loss after an initial decrease, and modern type III with steadily decreasing power loss (also see Fig. S1 within the Supplemental Material) [14]. Type II is under the transition stage between types I and III. Notably, the microscopic morphology, crystal structures, and chemical components among them are almost identical (see Fig. S2 within the Supplemental Material), in despite of the significant difference in aging performance [14]. It is hard to distinguish them from a structure aspect. Therefore, for further exploring the aging mechanism of DSB, types I and III should be specially focused and clear understandings on them need to be first established. Moreover, any proposed aging model must be suitable for all those three types of ZnO varistor ceramics simultaneously, due to their same aging nature [13].

*wukning@xjtu.edu.cn

†lijy@xjtu.edu.cn

‡These authors contributed equally to this work.

The traditional increase in power loss of ZnO varistor ceramics (type I) has been widely investigated, which could be well explained by the classic ion migration model [15,16]. It was reported that DSB comprises of negatively charged interface states and positively charged depletion layers [6,9,15]. The interface states were reported to associate with the interfacial defects created by dislocations between adjacent grains or impurity atoms trapped at the interface [6]. The depletion layers consist of cations like zinc interstitials and oxygen vacancies, compensating the negatively charged interface states [17,18]. If an external voltage was applied on the DSB, some mobile ions are driven towards the grain boundary and further combine with the interface states. Barrier height is thereby lowered down, which is exhibited as deteriorated electrical properties on the macroscopic scale, e.g., increased power loss, raised leakage current, and decreased nonlinear coefficient [19]. Results that were in support of the classic ion migration model have been reported with the development of experimental techniques [20,21]. Ion migration has been recognized as a fundamental physical scene for the aging of DSB.

However, the steadily decreasing power loss of ZnO varistor ceramics (type III) is beyond current understandings. In fact, it was already listed as a major future challenge by the International Council on Large Electric systems (CIGRE) in 2013 [12], again by CIGRE in 2017 [13]. The steady decrease in power loss was in direct contradiction to the classic ion migration model, which predicted a reduction in barrier height. A challenge appeared that any hypothesis proposed to explain the increase in barrier height during the aging process must be compatible with the classic ion migration model, although they seem to be conflicting [13]. Deep understandings on dynamics of ions in depletion layers of DSB under long-term aging were foundation to address this issue, which, as discussed above, was missing. The absence of a general aging mechanism of ZnO varistor ceramics, on the one hand, made it difficult to pertinently optimize the antidegradation performance. Electrical properties of ZnO varistor ceramics, as a kind of high-precision electronic ceramics, were sensitive to raw materials, sintering, and postannealing. Therefore, performance optimization largely depends on experience from tests. On the other hand, the declining amplitude of power loss increases at elevated temperatures, which no longer obeys the Arrhenius relationship. Condition assessment and life prediction of those modern type-III ZnO varistor ceramics could be hardly carried out because of lacking relevant physical basis. Apparently, a general understanding on the aging of DSB, which is able to explain all the aging types, is the first priority to further develop stable DSB and next-generation high-performance varistors.

In addition, only when species of the major mobile ions are identified could the aging mechanism be thoroughly revealed. Unfortunately, this issue is still in debate. Oxygen vacancies and zinc interstitials were all proposed as potential candidates [22]. Although zinc interstitials gained more and more acceptance due to the low migration energy of approximately 0.5 eV [18,21,23], debates appeared on whether $Zn_i^{\cdot}$ or $Zn_i^{\cdot\cdot}$ ions were the major mobile ions. The two zinc interstitials are basically originated from Frenkel defect reaction. Their major difference lies in the thermal transition levels, which have been reported as 0.05 and 0.20 eV below the conduction-band minimum (CBM) through broadband dielectric spectroscopy and deep-level transient spectroscopy techniques [22,24,25]. Gupta *et al.* suggested that both $Zn_i^{\cdot}$ and $Zn_i^{\cdot\cdot}$ ions were mobile ions [15]. Migration of $Zn_i^{\cdot}$ ions was employed by a number of researchers in their studies [23,26]. Meanwhile, improved antidegradation properties of ZnO varistor ceramics were also ascribed to decreased mobility of $Zn_i^{\cdot\cdot}$ ions [27–29]. By using an analytic method, He *et al.* excluded $Zn_i^{\cdot}$ ions from the list of candidates and further proposed that $Zn_i^{\cdot\cdot}$ ions from $V_o^{\times}$-$Zn_i^{\cdot\cdot}$ complex defects were the mobile ions [22]. The lack of consensus on such a basis issue makes it hard to quantify the dynamics of ions in depletion layers of DSB during aging, leaving the classic ion migration model still a qualitative theory.

In this paper, a comparative study on the aging of type-I and III ZnO varistor ceramics is carried out via both experiment and simulation. A quantitative dynamic ion migration-diffusion model is built. The unique decreasing power loss is found to arise from dynamics of mobile $Zn_i^{\cdot}$ ions in depletion layers with stable interface states. Variation of power loss during aging is essentially a result of completion between consumption of interface states and dynamics of mobile ions in depletion layers. The findings of this study unveil a general understanding on the aging of DSB and open avenues to manipulate the antidegradation performance of ZnO varistor ceramics.

II. EXPERIMENTS

In this paper, relatively harsh dc aging is performed on ZnO varistor ceramics. In addition, only samples of types I and III are investigated, because type II is the intermediate state between types I and III. A dc voltage, which is 0.8 times the breakdown voltage, is applied on the samples at 120 °C, during which the power loss is continuously recorded. The dc voltage is removed after the aging process. The samples are still placed in an oven at 120 °C for recovering. Nonlinear current density-electric field (J-E) characteristics in both forward and reverse directions are measured *in situ* during both the aging and recovering processes. In addition, samples at different aging and recovering stages are quickly cooled to −110 °C for frequency-domain dielectric spectroscopy (FDS) measurements. The offline tests of FDS are measured by an impedance analyzer (Novocontrol, Concept 80, Germany) at −110 °C from 10^{-1} to 10^{6} Hz with an ac signal of 1 Vrms.

Based on the measured J-E characteristics, nonlinear coefficient (α) is calculated as $\alpha = 1/\lg(U_{1\ \mathrm{mA}}/U_{0.1\ \mathrm{mA}})$, where $U_{1\ \mathrm{mA}}$ and $U_{0.1\ \mathrm{mA}}$ are voltages under 1 mA/cm^2 and 0.1 mA/cm^2, respectively. Breakdown field is defined as $E_b = U_{1\ \mathrm{mA}}/d$, where d is the thickness of samples. Leakage current density J_L is calculated as the current density at 0.75 $U_{1\ \mathrm{mA}}$.

Moreover, dc aging is conducted *in situ* on both type-I and type-III ZnO samples at room temperature in an impedance analyzer (Concept 80, Novocontrol, Germany) equipped with a high-voltage source module (HVB 4000). A dc voltage (0.8 $U_{1\ \mathrm{mA}}$ in amplitude) is first applied for 10 h and then set to zero for the next 15 h. Leakage current is continuously recorded during the aging process, while FDS is *in situ* monitored during both aging and recovering processes with an ac signal of 5 Vrms.

III. RESULTS AND DISCUSSIONS

A. dc aging and recovering of type-I ZnO ceramics

Figure 1(a) shows the monotonously increasing power loss with ongoing aging time of type-I ZnO varistor ceramics, which is in consistence with numbers of previous reports [11,15,16]. It fits well with the empirical equation $p \propto t^{1/2}$, where p is the power loss and t is the aging time. The nonlinear J-E characteristics in both forward and reverse directions are also measured and demonstrated in Figs. 1(b1) and 1(b2), respectively. The whole J-E curves in both forward and reverse directions move to the high-current range with increasing aging time. In addition, a severer deterioration in nonlinear J-E performance is observed in the reverse direction. Dependences of nonlinear coefficient (α), leakage current density (J_L), and breakdown electric field ($E_{1\ \mathrm{mA}}$) on aging time are shown in details in Fig. S3 within the Supplemental Material [14]. According to the classic ion migration model [15,22], interface states are combined with the mobile ions driven to the grain boundaries by the applied electric field, leading to the deformation of DSB, the rise in power loss, and the deterioration in electrical nonlinearity.

After the aging process, the samples are kept at the same temperature for recovering under a zero bias voltage. Figures 1(c1) and 1(c2) exhibit the J-E characteristics in forward and reverse directions during the recovering process, respectively. Apparently, the J-E curves move towards the lower current region with increasing

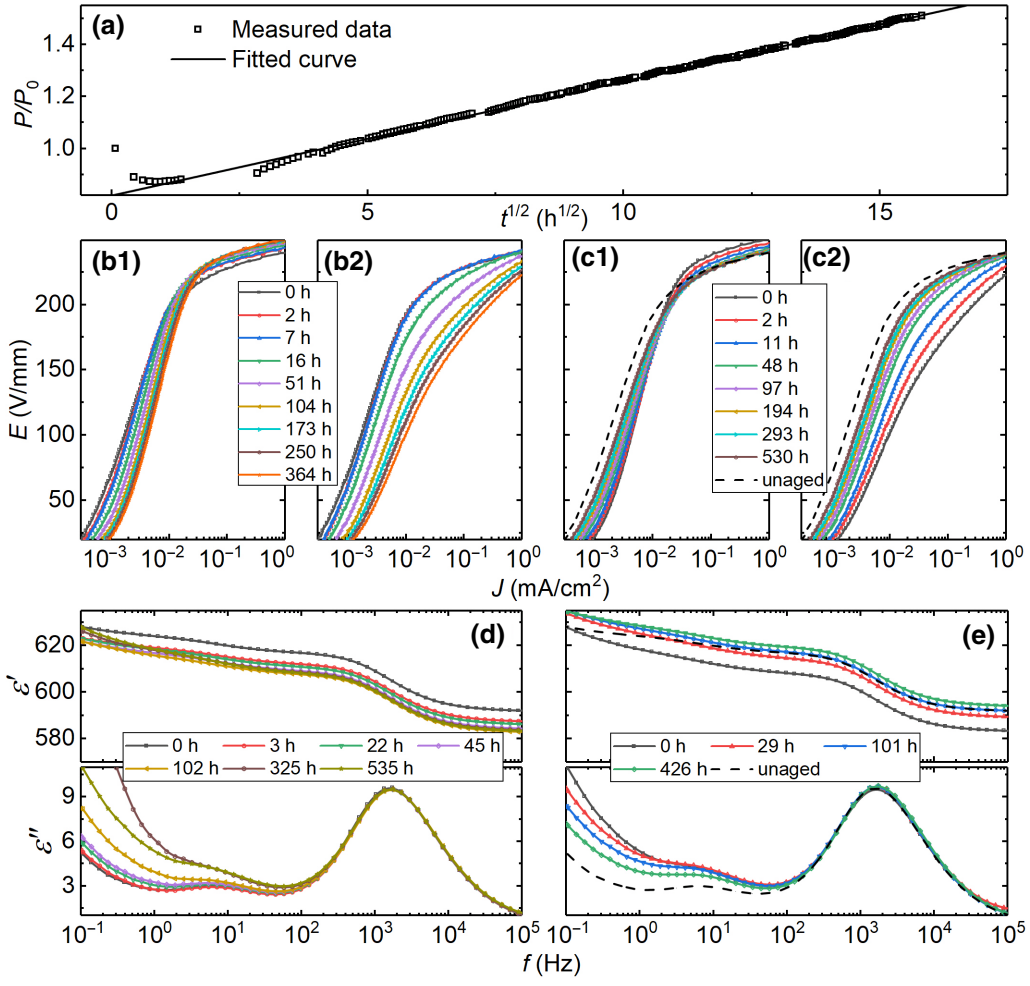

FIG. 1. Electrical properties of the type-I ZnO varistor ceramics. Steady increase in power loss (a). Nonlinear current-voltage characteristics in forward (b1) and reverse (b2) directions during aging process. Nonlinear current-voltage characteristics in forward (c1) and reverse (c2) directions during recovering process. FDS of the ZnO varistor ceramics at −100 °C during aging (d) and recovering (e).

recovering time, indicating that the recovering is a reverse process of the aging. Unfortunately, the J-E curves, even after 530 h of recovering, could not recover to their initial unaged states, due to the combination of interface states [15].

FDS results of the type-I ZnO varistor ceramics during the aging process are demonstrated in Fig. 1(d). The real part of complex permittivity ε' gradually declines with ongoing aging time. In addition, a rise in low-frequency loss is observed in the spectra of the imaginary part of complex permittivity ε''. As for the recovering process displayed in Fig. 1(e), ε' keeps rising up until it surpasses the unaged values, especially in the low-frequency range. Although a reduction in the low-frequency loss is detected, it is still much larger than the initial losses. The above results are in consistence with previous reports and can be well explained by the ion migration model [15,30]. It is not discussed further in this paper.

B. dc aging and recovering of type-III ZnO ceramics

Totally different aging phenomena are observed in type-III ZnO varistor ceramics, compared with those type-I samples. As displayed in Fig. 2(a), power loss of the type-III ZnO varstior ceramics steadily decreases with increasing aging time, which could be well fitted by double exponential function. Generally, the current density J flowing through a DSB follows [6,31]:

$$J = A^* T^2 e^{-\frac{e\phi_b + \xi_b}{kT}} (1 - e^{-\frac{eU}{kT}}), \tag{1}$$

where A^* is the effective Richard constant, k is the Boltzmann constant, T is the absolute temperature. ϕ_b is the barrier height under the applied voltage U. ξ_b is the bulk Fermi level relative to the conduction band. J is approximate to $A^* T^2 \exp[-e(\phi_b + \xi_b)/(kT)]$ when U is not too low. In other words, J is inversely correlated with ϕ_b. The detected decrease in power loss indicates that barrier height continuously rises, which is in contrast to the deformation of barrier predicted by the ion migration model.

Another unique aging phenomenon of type-III ZnO varistor ceramics is found on the J-E characteristics displayed in Fig. 2(b). With increasing aging time, the J-E curves in reverse direction shown in Fig. 2(b2) shift to higher current region as a whole, which is similar to the results of type-I samples. However, a "crossover" phenomenon appears for the J-E curves measured in the forward direction, as shown in Fig. 2(b1). The curves move towards a higher current region at low voltages, while they shift to a lower current region at high voltages. It indicates that, according to Eq. (1), the barrier height decreases at low voltages but increases at high voltages. The steady decrease in power loss in Fig. 2(a) is associated with the rise in barrier height at high voltages. Therefore, any model proposed to explain the rise in barrier height must be simultaneously compatible with the decrease in barrier height at low voltages.

Recovering of the samples is further conducted at the same aging temperature after the aging process. Figures 2(c1) and 2(c2) exhibit the nonlinear J-E characteristics of type-III ZnO varistor ceramics in forward and reverse directions, respectively, during the recovering process. With increasing recovering time, the curves move towards the initial ones. Remarkably, after 580 h of recovering, the J-E curves in both Figs. 2(c1) and 2(c2) almost totally overlap with the initial unaged J-E curves. This is also supported by the totally recovered α, $E_{1\,\mathrm{mA}}$, and J_L, which is shown in Fig. S4 within the Supplemental Material [14]. It is thus reasonable to deduce that aging of the type-III ZnO varistor ceramics is a completely reversible process, which differs to the irreversible aging of type-I samples shown in Fig. 1. This might shed light on the complex aging phenomenon of ZnO varistor ceramics. According to the classic ion migration model, the reduction in barrier height finally arises from consumption of interface states. Therefore, it is proposed that the interface states of the type-III samples should stay stable to maintain the aging as a reversible process. In other words, the unique phenomena might originate from redistribution of depletion layers, which is manipulated by stable interface states.

To further unveil the variation of depletion layers, FDS of the samples are measured at $-100\,^{\circ}\mathrm{C}$ during both aging and recovering processes, which are presented in Figs. 2(d) and 2(e), respectively. Similar to type-I ZnO varistor ceramics, permittivity and the relating loss peaks of the samples gradually decrease during aging due to the distortion of depletion layers [15,29]. They gradually lift up with increasing recovering time. Remarkably, FDS of the samples recovered for 370 h are identical to that of the unaged samples. The similar reversible FDS results further support the significance of stable interface states during the aging process despite the variation of depletion layers.

It should be pointed out that the unique reversible aging of type-III ZnO varistor ceramics makes it possible to further study dynamics of the intrinsic point defects in depth. Based on the assumption that interface states remain stable, variation of FDS arises only from dynamics of the intrinsic point defects in depletion layers. As a powerful technique, electron trapping of the point defects can be characterized as dielectric relaxations in FDS [32–34]. Generally speaking, the high-frequency peak and the low-frequency peak in ε'' spectra in Fig. 2(d) are reported to correlate with electron trapping of $Zn_i^{\cdot\cdot}$ and $V_o^{\cdot}$, respectively [35,36]. In addition, the high-frequency permittivity of the ZnO ceramic samples is in the hundreds, which is much larger than the optical permittivity of ZnO (8.5). Another relaxation peak would further appear in the radio-frequency range (see Fig. S5 within the Supplemental Material) [14].

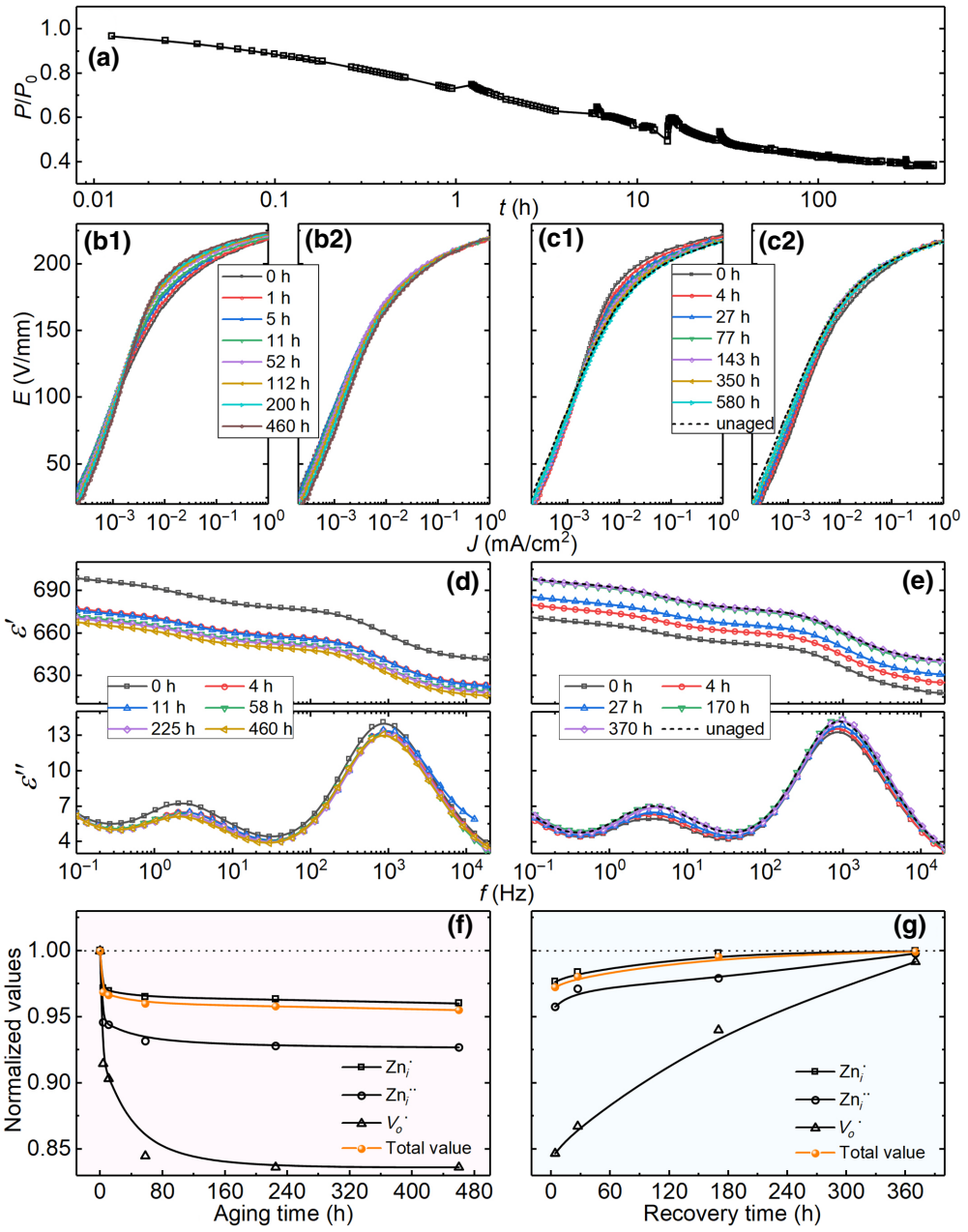

FIG. 2. Electrical properties of the type-III ZnO varistor ceramics. Steady decrease in power loss during aging (a). Nonlinear current-voltage characteristics in forward (b1) and reverse (b2) directions during the dc aging process. Nonlinear current-voltage characteristics in forward (c1) and reverse (c2) directions during recovering process. FDS of the ZnO varistor ceramics at −100 °C during the aging (d) and recovering (e). Dependence of relaxation magnitudes on aging time (f) and recovering time (g).

Its relaxation activation energy is calculated to be 0.04 eV (see Fig. S6 within the Supplemental Material), which is in accordance with the reported trap depth of $Zn_i^{\cdot}$ [14,17,37]. Therefore, magnitudes of those relaxations, which represent electron trappings of $Zn_i^{\cdot}$, $Zn_i^{\cdot\cdot}$, and $V_o^{\cdot}$ respectively, could be obtained by fitting the FDS results via the Cole-Cole equation for further investigation [38–40]. The details of fitting are shown in Fig. S7 within the Supplemental Material [14].

Generally, the total permittivity containing all those relaxations is proportional to the width of depletion layers, because the measured overall capacitance is the barrier capacitance. In addition, magnitude of a dielectric relaxation from electron trapping of point defect in depletion layers follows [34,35,41]:

$$C_i = \frac{N_{ti}}{n}\frac{\omega^2}{1+\omega^2\tau^2}\left(\frac{\varepsilon_0\varepsilon_r e N_d}{2\phi_b}\right)^{1/2}, \qquad (2)$$

where C_i is the capacitance contributed by the ith donor point defects, N_{ti} is the ith donor density, N_d is the positive space-charge density in depletion layers, and n is the free electron density. Magnitudes of all the relaxations decrease with increasing aging time, due to distortion of depletion layers. It is hard to directly compare their absolute variation, because of the large differences in base. Therefore, the magnitude of each relaxation during the aging process is normalized to its initial value, as exhibited in Fig. 2(f).

The curve corresponding to $Zn_i^{\cdot}$ and curves corresponding to $Zn_i^{\cdot\cdot}$ and $V_o^{\cdot}$ locate on upside and downside of the curve corresponding to the total permittivity, which represents distortion of depletion layers as a whole. The results clearly suggest that distortion of depletion layers is mainly manipulated by migration of $Zn_i^{\cdot}$ ions. Similar phenomena are also found in the recovering process. Normalized magnitudes of the relaxations to their final stable values are shown in Fig. 2(g), where only the curve corresponding to $Zn_i^{\cdot}$ locates on the upside.

According to Eq. (2), magnitudes of the relaxations are proportional to their corresponding donor densities under the identical state. Proportion of a donor defect $P_i (i = Zn_i^{\cdot}, Zn_i^{\cdot\cdot}$, and $V_o^{\cdot})$ is able to be calculated. Ratio of P_i to its initial value P_{i0} is further calculated to characterize the evolution of each point defect during aging (see Figs. S8 and S9 within the Supplemental Material) [14]. In fact, only the ratio of $Zn_i^{\cdot}$ increases while ratios of $Zn_i^{\cdot\cdot}$ and $V_o^{\cdot}$ decrease during the aging process. Similarly, only the ratio of $Zn_i^{\cdot}$ decreases while ratios of both $Zn_i^{\cdot\cdot}$ and $V_o^{\cdot}$ increase during the recovering process. Apparently, all the results above indicate that $Zn_i^{\cdot}$ ions are the major mobile ions in ZnO varistor ceramics. Therefore, the intrinsic point defect $Zn_i^{\cdot}$ should be specifically focused.

C. *In situ* aging and recovering

Almost all the studies on the aging of ZnO varistors were carried out on the basis of offline tests, because of the harsh conditions, e.g., the long duration time, the high temperature and the high aging voltage. Particularly, it is rather hard to characterize the real-time distortion of depletion layers of the DSB, because free electrons are quickly trapped by those point defects at the edge of depletion layers [32,34,37]. It is notable that the major reduction in power loss of type-III ZnO samples in Fig. 2 appears in only 5 h. This makes it possible to *in situ* investigate the dc aging of ZnO varistor ceramics directly by an impedance analyzer. The capacitance and leakage current of the type-III samples are simultaneously recorded during the aging at room temperature, as plotted in Fig. 3(b). Steady decrease in leakage current density is clearly observed in the inset of Fig. 3(b). It is accordant with steadily decreased power loss that measured at elevated temperature of 120 °C, indicating the same aging mechanism. Similar results are also found in type-I ZnO varistor ceramics. The increasing leakage current density shown in the inset of Fig. 3(a) is in line with the increasing power loss shown in Fig. 1(a). Therefore, it is effective to *in situ* characterize the evolution of depletion layers during aging merely by monitoring the permittivity, as demonstrated in Fig. 3.

When an external voltage is applied, the permittivity of both type-I and III ZnO varistor ceramics steadily decreases after an initial dramatic reduction. The sharp reduction in permittivity arises from electron filling of interface states, leading to dramatic extension of depletion layers [6]. This process is so fast that it can be completed in less than 1 s at such a high voltage [34], which is also simulated and shown in Fig. S10 within the Supplemental Material [14]. The subsequent steady decrease in permittivity, indicating a continuously extension in depletion layer width, could only originate from migration of $Zn_i^{\cdot}$ ions. $Zn_i^{\cdot}$ ions are forced to migrate towards the grain boundary because of a strengthened electric field in the reversed depletion layer of DSB. This process further strengthens the electric field and drives more $Zn_i^{\cdot}$ ions into depletion layers. It is in accordance with the classic ion migration model.

Significant discrepancies between type-I and III samples appear in the recovering process. When the applied voltage is removed, permittivity of both samples dramatically lifts up in the initial stage and then steadily increases, which are ascribed to electron emission of interface states and migration of $Zn_i^{\cdot}$ ions, respectively. Notably, permittivity of type-I ZnO samples shown in Fig. 3(a) quickly exceeds the initial permittivity, while permittivity of type-III samples in Fig. 3(b) is almost identical to the initial one. Never does it happen that permittivity grows higher than the initial value. According to the classic ion migration model, the increased permittivity of type-I ZnO varistor ceramics originates from combination of interface states, which leads to reduced interfacial charge and extended depletion

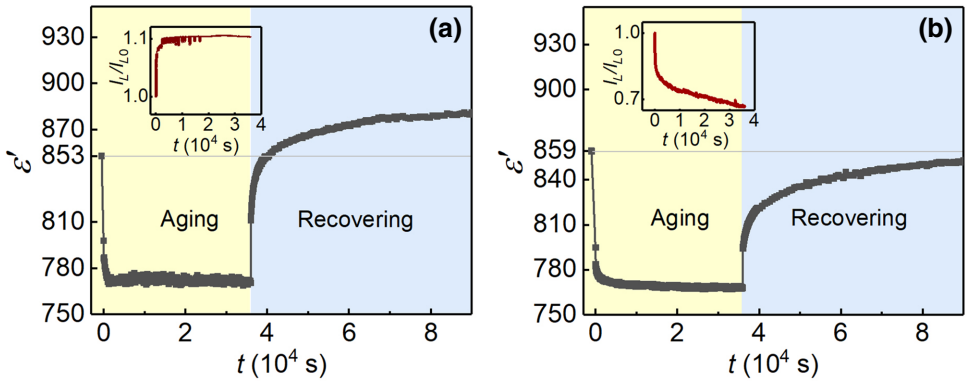

FIG. 3. Permittivity (10^4 Hz) measured *in situ* during aging and recovering of type-I (a) and type-III (b) ZnO ceramics at room temperature. Insets are corresponding leakage current curves during aging.

layers. Therefore, results of *in situ* aging and recovering of type-III ZnO ceramics further prove it a completely reversible process in which stable interface states are of significance.

D. Simulation of the long-term dc aging

It can be concluded from above discussions that dynamics of $Zn_i^{\cdot}$ ions and electron trapping of interface states should take responsibility for the unique aging phenomena of type-III varistor ceramics, with stable interface states as a premise. When a voltage is applied on a DSB, initial dynamic balance of depletion layers collapses. Mobile $Zn_i^{\cdot}$ ions are driven by the strengthened electric field to the interface but not combined with the interface states. Electron trapping of the interface states consequently takes place to balance the distortion of deletion layers, leading to redistribution of electric field in the DSB. This further affects migration of $Zn_i^{\cdot}$ ions and distortion of depletion layers. Apparently, dc aging of ZnO varistor ceramics involves complex interaction between ion migration and electron trapping of interface states that one has to seek help from numerical simulation. Following the classic hypothetico-deductive method, the aging mechanism of type-III ZnO varistor ceramics is able to be unveiled if the simulated results fitted well with all the measured data. A flow diagram of simulation is shown in Fig. S11 within the Supplemental Material [14].

First, a mathematical model of DSB is built on the basis of Blatter and Greuter's DSB model [6]. In this paper, interface states that follow Gauss distribution are fixed at 1.2 eV below the conduction band. The major mobile $Zn_i^{\cdot}$ ions are also the dominant donors in ZnO [18]. Therefore, depletion layers are set to comprise only of $Zn_i^{\cdot}$ ions for simplicity. The only problem left is to correlate the interfacial charge Q_i and the barrier height ϕ_b to the applied voltage U. ϕ_b follows Poisson's equation, which depends on the ion distribution in depletion layers. Q_i, on the one hand, is equal to depletion layer charge due to charge conservation:

$$Q_i = Q_{\mathrm{DF}} + Q_{\mathrm{DR}}, \tag{3}$$

where Q_{DF} and Q_{DR} are charge of forward- and reverse-biased depletion layer, respectively. On the other hand, Q_i obeys the Fermi distribution:

$$Q_i = e\int_{\xi_i^n}^{\infty} N_i(E) f_i(E) dE, \tag{4}$$

with

$$f_i(E) = \frac{1}{1 + e^{E-\xi_i(U)}/kT}, \tag{5}$$

$$\xi_i(U) = \xi_b + e\phi_b(U) + \Delta\xi_i(U), \tag{6}$$

where $N_i(E)$ is density of interface states and $f_i(E)$ is the Fermi distribution. $\xi_i(U)$ is the (quasi-)Fermi-level of the interface under applied voltage U, ξ_b is the position of bulk Fermi level, $\Delta\xi_i$ is the shift of ξ_i. The close relation among ϕ_b, Q_i, and U makes it impossible to be analytically solved, as long as positively charged ions are not uniformly distributed in depletion layers [6,34]. In this paper, the complicated issue is solved by using the genetic algorithm, in which ϕ_b is the optimized variable, the law of charge conservation is objective constraints. Voltage-dependent barrier height of a DSB with the same conditions in Ref. [6] is shown in Fig. S12 within the Supplemental Material as an example, which verifies feasibility of this method [14].

Secondly, redistribution of ions in depletion layers induced by ion migration is calculated by migration-diffusion equations. When the external voltage is applied on the DSB, $Zn_i^{\cdot}$ ions initially in dynamic equilibrium would migrate along electric field. The migration rate ΔN_d follows [42]:

$$\Delta N_d = \frac{N_{d0}}{6}\nu e^{-\frac{u_0}{kT}}(e^{\Delta u/kT} - e^{-\Delta u/kT}), \tag{7}$$

with mobility

$$\mu = \frac{\delta}{6E}\nu e^{-\frac{u_0}{kT}}(e^{\frac{\Delta u}{kT}} - e^{-\frac{\Delta u}{kT}}), \tag{8}$$

where N_{d0} is the initial donor concentration, ν is the ion vibration frequency, u_0 is the migration barrier height at zero bias, δ is the average distance between two adjacent barrier traps, and Δu is the potential drop induced by electric field that can be written as $\Delta u = eE\delta/2$. The current density caused by migration part can be written as

$$J_E = eN_d\mu E. \tag{9}$$

In addition, diffusion flux is formed as long as concentration gradient of $Zn_i^{\cdot}$ ions is not zero:

$$J_D = -D\frac{\partial N_d}{\partial x}, \tag{10}$$

where D is the diffusion coefficient that satisfies the Einstein relationship $D/\mu = kT/e$ and $N_d(x,t)$ is the donor concentration. Consequently, density of $Zn_i^{\cdot}$ ions at any time t and position x can be expressed as

$$\frac{\partial N_d(x,t)}{\partial t} + \frac{\partial J_E(x,t) + \partial J_D(x,t)}{\partial x} = 0. \tag{11}$$

Monotone upstream-centered schemes for conservation laws (MUSCL) method with the limit function of Koren is employed to solve Eq. (11), because it can provide stable and high-order accurate numerical charge-distribution results [22].

Long-term aging of a DSB is consequently obtained by continuously iterating and updating the above two processes. It was reported that gradients of ion spatial distribution in unaged ZnO varistor ceramics are minimal, because of the high-temperature sintering and later cooling process [9]. Therefore, in this paper, constant density N_{d0} of 1.0×10^{24} m^{-3} is employed in the initial unaged DSB. In addition, a maximum value of ion concentration is introduced because there is definitely a physical limit in ion density, which is set to $2N_{d0}$ in this simulation. If the ion concentration at the grain boundary reached $2N_{d0}$, excess migrating ions are set to accumulate at the grain boundary. Breakdown voltage of the DSB is calculated to be about 4 V, so that a dc voltage of 3.2 V is applied on the DSB to calculate its long-term responses. A list of parameters that are involved in the simulation in detail are shown in Table S1 within the Supplemental Material [14].

The simulated leakage current density J_L and barrier capacitance C during the aging are shown in Fig. 4(a). The J_L, proportional to the power loss, drops sharply in the first 10 h and steadily decreases in the following time, which fits well with the measured power loss presented in Fig. 2(a). According to Eq. (1), the decreasing leakage current density essentially originates from the increasing barrier height. As shown in Fig. 4(b), ϕ_b gradually increases from the initial approximately 0.89 eV to approximately 0.91 eV after aging. The increase in ϕ_b, according to Eq. (4), results in a slightly decrease in interfacial charge Q_i, which is also plotted in Fig. 4(b). Apparently, a higher barrier height is built by less space charges in depletion layers, which are equal to Q_i according to Eq. (3). In accordance with the *in situ* aging results in Fig. 3(b), the calculated barrier capacitance C also declines with increasing aging time [dramatic reduction in C from electron filling of the interface states is separately shown in Fig. S10(c) within the Supplemental Material] [14]. All those results suggest that the ion spatial distribution in the depletion layers plays a significant role in the aging of type-III ZnO varistor ceramics.

Distortion of depletion layers caused by the migration-diffusion process during the aging is exhibited in Fig. 4(c). Severer distortion is found in the reverse-biased depletion layer, which mainly bears the applied voltage. Driven by the electric field, $Zn_i^{\cdot}$ ions migrate to and accumulate at

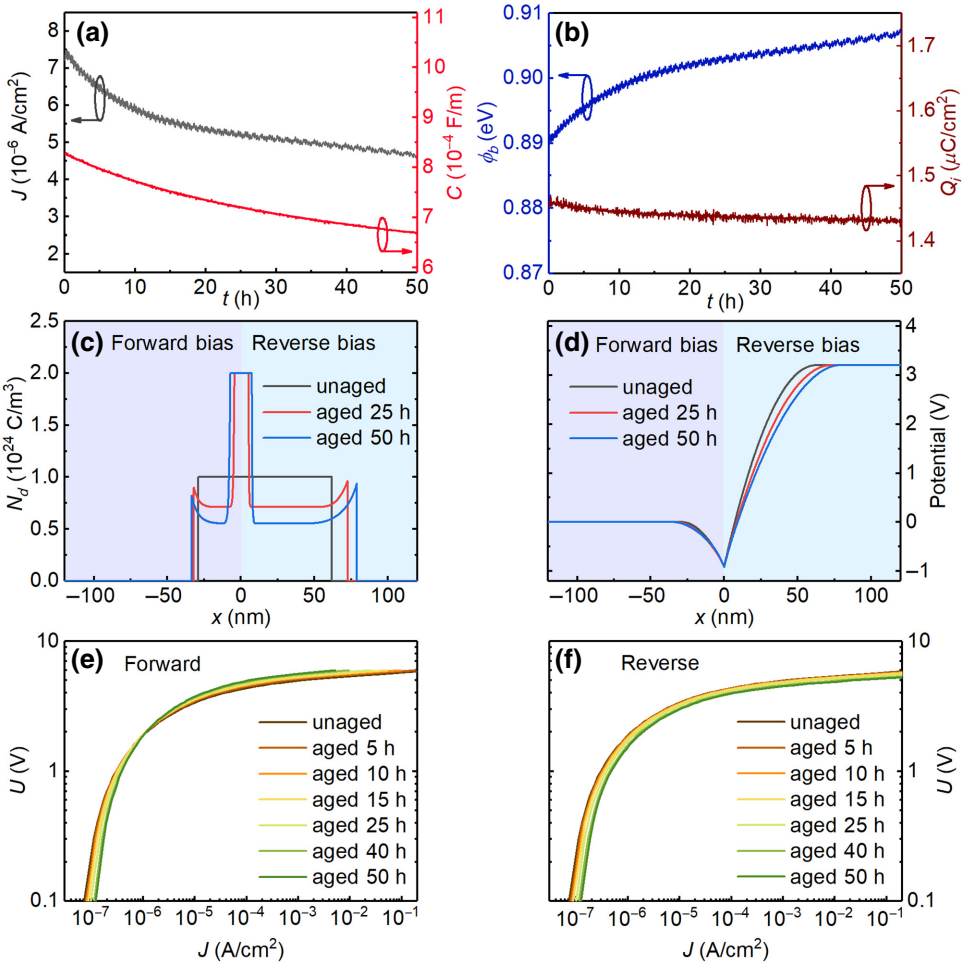

FIG. 4. Evolution of leakage current (a), barrier height ϕ_b and interface charge Q_i (b), bulk donor distribution (c), and potential distribution (d) in the long-term dc aging simulation of a single grain boundary. Nonlinear J-E characteristics in forward (e) and reverse (f) directions.

grain boundaries. As a result, a "U-shape" ion distribution in the depletion layer is formed. Density of $Zn_i^{\cdot}$ ions reaches the maximum limit of $2N_{d0}$ at the grain boundary, drops to only approximately $0.5N_{d0}$ in the middle depletion layer, and slowly lifts up at the edge of the depletion layer. According to Poisson's equation, potential distribution of the depletion layer is calculated and plotted in Fig. 4(d). Based on this kind of specific spatial distribution of $Zn_i^{\cdot}$ ions in depletion layers, a higher barrier height is achieved with less depletion layer charges in total. As a result, electric fields at the edge of depletion layers are steadily strengthened during the aging process (see Fig. S13 within the Supplemental Material) [14]. The reverse-biased depletion layer thereby gradually extends itself by driving more $Zn_i^{\cdot}$ ions from grains into depletion layers to compensate the large density reduction in the middle depletion layers.

Furthermore, on the basis of distributions of $Zn_i^{\cdot}$ ions at different aging stages, nonlinear J-E characteristics of the DSB in both forward and reverse directions are simulated and plotted in Figs. 4(e) and 4(f), respectively. An obvious "crossover" phenomenon in the forward direction and overall shift to the high-current region in the reverse direction are observed, which exactly coincide with the experimental results in Fig. 2(b). It is thereby unveiled that "crossover" phenomenon is just an explicit characteristic of the implicit dynamic conservation between the interfacial charge and the depletion layer charge under varied applied voltages. The key is that specific distributions of $Zn_i^{\cdot}$ ions shown in Fig. 4(c) with stable interface states is formed under dc voltages. Decreased barrier height and increased leakage current would be observed as long as the aging voltage is low enough. In other words, it is predictable that power loss of the same type-III ZnO varistor ceramics would steadily increase rather than decrease, if a relatively low dc aging voltage, e.g., 0.3 $U_{1\ \mathrm{mA}}$, is applied.

Additionally, for the recovering process, when the applied voltage is removed, the electric field strength in depletion layers transiently decreases. According to Eq. (10), the diffusion flux overwhelms the weakened migration flux instantly due to the dramatic concentration gradients in the "U-shape" ion distribution. The accumulated $Zn_i^{\cdot}$ ions at grain boundaries then diffuse into grains, which is accompanied by electron filling of interface states. Eventually, the barrier height recovers to its initial height and the samples regain their electrical properties. More experiments and simulations on the recovering process are needed.

IV. CONCLUSIONS

In conclusion, this study focuses on the aging mechanism of the type-III ZnO varistor ceramics whose steadily decreasing power loss is contradictory to the prediction of the classic ion migration model. For those type-III ZnO varistor ceramics, a "crossover" phenomenon appears on their current-voltage characteristics, i.e., the leakage current increased at low voltages but declined at high voltages. Furthermore, another distinctive feature of type-III ZnO varistor ceramics is found that they could totally recover to their initial unaged state as long as the external voltage is removed. Based on this feature, stable interface states are proposed to be of significance and the major mobile ions are identified to be $Zn_i^{\cdot}$ ions. Following the classic hypothetico-deductive method, we, with the help of numerical simulation, unveil that the steadily decreasing power loss originates from the elevated barrier height essentially arose from dynamics of mobile ions at the external voltage. Mobile $Zn_i^{\cdot}$ ions are forced to migrate from depletion layers to the grain boundary but not combined with the interface states under the dc bias. As a result, a "U-shape" distribution of ion density is formed in depletion layers, i.e., ion density lifted up at the grain boundary, dropped down in the middle depletion layers, and slightly went up again at the edge of depletion layers. All the observed aging phenomena are explicit electrical responses of the implicit dynamic conservation between interfacial charge and depletion layer charge at applied voltages. Once sufficient interface states are combined with mobile ions, reduction in barrier height and continuous increase in power loss would be detected in those type-I and II ZnO varistor ceramics. A general understanding is gained that aging of DSB is a competition between consumption of interface states and dynamics of mobile ions in depletion layers, which lays the groundwork for future research into performance optimization and condition assessment of modern ZnO varistor ceramics. In addition, future investigations into interactions among different point defects ($Zn_i^{\cdot}$, $Zn_i^{\cdot\cdot}$, $V_o^{\cdot}$, and others) and the reason why interface states could maintain themselves are recommended.

ACKNOWLEDGMENTS

This work is supported by the National Natural Science Foundation of China (Grants No. 52107027, No. 51937008). K.W. is grateful to the great support of Ms. Lu Hua.

[1] P. K. Nayak, S. Mahesh, H. J. Snaith, and D. Cahen, Photovoltaic solar cell technologies: Analysing the state of the art, Nat. Rev. Mater. **4**, 269 (2019).

[2] J. Pipek, M. Betušiak, E. Belas, R. Grill, P. Praus, A. Musiienko, J. Pekarek, U. N. Roy, and R. B. James, Charge Transport and Space-Charge Formation in $Cd_{1-x}Zn_xTe_{1-y}Se_y$ Radiation Detectors, Phys. Rev. Appl. **15**, 054058 (2021).

[3] X. Lu, L. Zhou, L. Chen, X. Ouyang, B. Liu, J. Xu, and H. Tang, Schottky x-ray detectors based on a bulk β-Ga_2O_3 substrate, Appl. Phys. Lett. **112**, 103502 (2018).

[4] P. Keil, M. Trapp, N. Novak, T. Frömling, H.-J. Kleebe, and J. Rödel, Piezotronic tuning of potential barriers in ZnO bicrystals, Adv. Mater. **30**, 1705573 (2018).

[5] D. Gedamu, I. Paulowicz, S. Kaps, O. Lupan, S. Wille, G. Haidarschin, Y. K. Mishra, and R. Adelung, Rapid fabrication technique for interpenetrated ZnO nanotetrapod networks for fast UV sensors, Adv. Mater. **26**, 1541 (2014).

[6] G. Blatter and F. Greuter, Carrier transport through grain boundaries in semiconductors, Phys. Rev. B **33**, 3952 (1986).

[7] T. Tian, L. Zheng, M. Podlogar, H. Zeng, S. Bernik, K. Xu, X. Ruan, X. Shi, and G. Li, Novel ultrahigh-performance ZnO-based varistor ceramics, ACS Appl. Mater. Inter. **13**, 35924 (2021).

[8] Z. Tang, K. Ning, Z. Fu, K. Wu, and S. Huang, Significantly enhanced varistor properties of $CaCu_3Ti_4O_{12}$ based ceramics by designing superior grain boundary: Deepening and broadening interface states, J. Mater. Sci. Technol. **108**, 82 (2022).

[9] F. Greuter, ZnO varistors: From grain boundaries to power applications, Oxide Electronics, 157 (2021).

[10] P. Bueno, E. Leite, M. Oliveira, M. Orlandi, and E. Longo, Role of oxygen at the grain boundary of metal oxide varistors: A potential barrier formation mechanism, Appl. Phys. Lett. **79**, 48 (2001).

[11] K. Eda, Zinc oxide varistors, IEEE Electr. Insul. Mag. **5**, 28 (1989).

[12] CIGRE Working Group A3.17 (convenor B. Richter), *MO Surge Arresters - Stresses and Test Procedure* (Cigre Technical Brochure 544, 2013).

[13] CIGRE Working Group A3.25 (convenor B. Richter), *MO Surge Arresters - Metal Oxide Varistors and Surge Arresters for Emerging System Conditions* (Cigre Technical Brochure 696, 2017).

[14] See Supplemental Material at http://link.aps.org/supplemental/10.1103/PhysRevApplied.17.034042 for the evolution of electrical parameters during aging and recovering and the simulation process in detail.

[15] T. K. Gupta and W. G. Carlson, A grain-boundary defect model for instability/stability of a ZnO varistor, J. Mater. Sci. **20**, 3487 (1985).

[16] J. He, C. Cheng, and J. Hu, Electrical degradation of double-Schottky barrier in ZnO varistors, AIP Adv. **6**, 030701 (2016).

[17] D. C. Look, J. W. Hemsky, and J. R. Sizelove, Residual Native Shallow Donor in ZnO, Phys. Rev. Lett. **82**, 2552 (1999).

[18] A. Janotti and C. G. Van de Walle, Native point defects in ZnO, Phys. Rev. B **76**, 165202 (2007).

[19] K.-H. Bäther, W. Brückner, W. Moldenhauer, and H.-P. Brückner, Microscopic degradation model for ZnO varistors, Phys. Status Solidi A **75**, 465 (1983).

[20] C. Cheng, J. He, and J. Hu, Observation of the charged defect migration that causes the degradation of double-Schottky barriers using a nondestructive quantitative profiling technique, Appl. Phys. Lett. **105**, 133508 (2014).

[21] K. Ferri, E. A. Paisley, C. DiAntonio, S.-W. Han, R. Chu, and J.-P. Maria, Investigation of phase evolution within ZnO-Bi_2O_3 varistors utilizing thin film prototypes, J. Mater. Sci. **56**, 12740 (2021).

[22] J. He, C. Cheng, and J. Hu, An analytic approach to the degradation of double-Schottky barrier: Theoretical prediction of V_O^0–Zn_i^{2+}: Zn_i^{2+} as dominant mobile ion in ZnO electroceramic, Scripta Mater. **104**, 25 (2015).

[23] E. Leite, J. A. Varela, and E. Longo, A new interpretation for the degradation phenomenon of ZnO varistors, J. Mater. Sci. **27**, 5325 (1992).

[24] T. K. Gupta, Application of zinc oxide varistors, J. Am. Ceram. Soc. **73**, 1817 (1990).

[25] J. Han, A. Senos, and P. Mantas, Deep donors in polycrystalline Mn-doped ZnO, Mater. Chem. Phys. **75**, 117 (2002).

[26] P. Meng, X. Zhao, Z. Fu, J. Wu, J. Hu, and J. He, Novel zinc-oxide varistor with superior performance in voltage gradient and aging stability for surge arrester, J. Alloy. Compd. **789**, 948 (2019).

[27] J. Lin, S. Li, J. He, L. Zhang, W. Liu, and J. Li, Zinc interstitial as a universal microscopic origin for the electrical degradation of ZnO-based varistors under the combined dc and temperature condition, J. Eur. Ceram. Soc. **37**, 3535 (2017).

[28] M. Takada and S. Yoshikado, Effect of thermal annealing on electrical degradation characteristics of Sb-Bi-Mn-Co-added ZnO varistors, J. Eur. Ceram. Soc. **30**, 531 (2010).

[29] M. Wang, X. Ren, Q. Zhou, Z. Li, H. Yang, H. Jiang, Y. Yan, X. Ruan, W. Yu, and L. Jin, *et al.*, High improvement of degradation behavior of ZnO varistors under high current surges by appropriate Sb_2O_3 doping, J. Eur. Ceram. Soc. **41**, 436 (2021).

[30] K. Eda, A. Iga, and M. Matsuoka, Degradation mechanism of non-ohmic zinc oxide ceramics, J. Appl. Phys. **51**, 2678 (1980).

[31] G. Pike and C. H. Seager, The DC voltage dependence of semiconductor grain-boundary resistance, J. Appl. Phys. **50**, 3414 (1979).

[32] Y. Huang, K. Wu, Z. Xing, C. Zhang, X. Hu, P. Guo, J. Zhang, and J. Li, Understanding the validity of impedance and modulus spectroscopy on exploring electrical heterogeneity in dielectric ceramics, J. Appl. Phys. **125**, 084103 (2019).

[33] J. R. Macdonald and W. B. Johnson, *Impedance Spectroscopy: Theory, Experiment, and Applications, Third Edition* (John Wiley & Sons, Ltd, Hoboken, NJ, USA, 2018).

[34] K. Wu, Y. Wang, Z. Hou, S. Li, J. Li, Z. Tang, and Y. Lin, Colossal permittivity due to electron trapping behaviors at the edge of double Schottky barrier, J. Phys. D: Appl. Phys. **54**, 045301 (2020).

[35] J. F. Cordaro, Y. Shim, and J. May, Bulk electron traps in zinc oxide varistors, J. Appl. Phys. **60**, 4186 (1986).

[36] P. Cheng, S. Li, L. Zhang, and J. Li, Characterization of intrinsic donor defects in ZnO ceramics by dielectric spectroscopy, Appl. Phys. Lett. **93**, 012902 (2008).

[37] J. Han, A. Senos, P. Mantas, and W. Cao, Dielectric relaxation of shallow donor in polycrystalline Mn-doped ZnO, J. Appl. Phys. **93**, 4097 (2003).

[38] M. Guo, Y. Wang, K. Wu, L. Zhang, X. Zhao, Y. Lin, and J. Li, Revisiting the effects of Co_2O_3 on multiscale

defect structures and relevant electrical properties in ZnO varistors, High Volt. **5**, 241 (2020).

[39] T. Schenk, M. Hoffmann, M. Pešić, M. H. Park, C. Richter, U. Schroeder, and T. Mikolajick, Physical Approach to Ferroelectric Impedance Spectroscopy: The Rayleigh Element, Phys. Rev. Appl. **10**, 064004 (2018).

[40] K. Wu, Y. Huang, J. Li, and S. Li, Space charge polarization modulated instability of low frequency permittivity in $CaCu_3Ti_4O_{12}$ ceramics, Appl. Phys. Lett. **111**, 042902 (2017).

[41] L. Kimerling, Influence of deep traps on the measurement of free-carrier distributions in semiconductors by junction capacitance techniques, J. Appl. Phys. **45**, 1839 (1974).

[42] K. C. Kao, *Dielectric Phenomena in Solids* (Academic Press, Elsevier, San Diego, CA, USA, 2004), 381.